ELECTRIC FIELD AND STRAIN EFFECTS ON SURFACE ROUGHNESS INDUCED SPIN RELAXATION IN SILICON FIELD-EFFECT TRANSISTORS

Dmitri Osintsev[a,b], Oskar Baumgartner[a], Zlatan Stanojevic[a], Viktor Sverdlov[a], and Siegfried Selberherr[a]

[a]Institute for Microelectronics, TU Wien, Gußhausstraße 27-29, A-1040 Wien, Austria
[b]Volgograd State Technical University, Lenin Avenue 28, 400131 Volgograd, Russia

Email: {Osintsev|Baumgartner|Stanojevic|Sverdlov|Selberherr}@iue.tuwien.ac.at

ABSTRACT

Spintronics attracts at present much interest because of the potential to build novel spin-based devices which are superior to nowadays charge-based devices. Utilizing spin properties of electrons opens great opportunities to reduce device power consumption in future electronic circuits. Silicon, the main element of microelectronics, is also promising for spin-driven applications. Understanding the details of the spin propagation in silicon structures is a key for novel spin-based applications. We investigate the surface roughness induced spin relaxation in a silicon-on-insulator-based spin field-effect transistors for various parameters including the potential barrier at the interfaces, the film thickness, and shear strain. Shear strain dramatically influences the spin opening a new opportunity to boost spin lifetime in a silicon spin field-effect transistor.

Keywords: spin relaxation, **k·p** model, shear strain, surface roughness, spin MOSFET

1. INTRODUCTION

Since modern microelectronic devices are near to their fundamental scaling limits, a further boost of their performance could be eventually provided by changing their operational principles. Promising results have been already obtained by utilizing the spin properties of electrons. In order to achieve significant advantages by utilizing spin, materials possessing a long spin life-time and low relaxation rate must be used.

Silicon is the primary material for micro-electronics. The long spin life time in silicon is a consequence of the weak spin-orbit interaction and the spatial inversion symmetry of the lattice (Li and Appelbaum 2011, Li and Dery 2011). In addition, silicon is composed of nuclei with predominantly zero magnetic moment. A long spin transfer distance of conduction electrons has already been demonstrated experimentally (Huang, Monsma, Appelbaum 2007). Spin propagation at such distances combined with a possibility of injecting spin at room (Dash, Sharma, Patel, de Jong, Jansen 2009) or even elevated (Li, Van't Erve, Jonker 2011) temperature in silicon makes the fabrication of spin-based switching devices quite plausible in the upcoming future. However, the relatively large spin relaxation experimentally observed in electrically-gated lateral-channel silicon structures (Li and Appelbaum 2011) might become an obstacle in realizing spin driven devices (Li and Dery 2011), and a deeper understanding of the fundamental spin relaxation mechanisms in silicon is urgently needed (Song and Dery 2012).

In this work we investigate the influence of the intrinsic spin-orbit interaction on the subband structure, subband wave functions, and spin relaxation matrix elements due to the surface roughness scattering in thin silicon films. Following Li and Dery (Li and Dery 2011), a **k·p** approach (Bir and Pikus 1974, Sverdlov 2011) suitable to describe the electron subband structure in the presence of strain is generalized to include the spin degree of freedom.

In contrast to Li and Dery (Li and Dery 2011), our effective 4x4 Hamiltonian considers only relevant [001] oriented valleys with spin included, which produce the low-energy unprimed subband ladder. Within this model the unprimed subbands in the unstrained (001) film are degenerate without spin-orbit effects included. An accurate inclusion of the spin-orbit interaction results in a large mixing between the spin-up and spin-down states, resulting in spin hot spots along the [100] and [010] axes characterized by strong spin relaxation due to the spin-orbit coupling. These hot spots should be contrasted with the spin hot spots appearing in the bulk system (Cheng, Wu, Fabian 2010, Li and Dery 2011). Their origin lies in the unprimed subband degeneracy in a confined electron system which effectively projects the bulk spin hot spots at the edge of the Brillouin zone to the center of the 2D Brillouin zone.

Shear strain lifts the degeneracy between the unprimed subbands (Sverdlov 2011). The energy splitting between the otherwise equivalent subbands removes the origin of the spin hot spots in a confined silicon system, which should substantially improve the spin lifetime in gated silicon systems.

2. METHOD

We solve numerically the Hamiltonian

$$H = \begin{bmatrix} H_1 & H_3 \\ H_3^{\dagger} & H_2 \end{bmatrix} \quad (1)$$

with H_1, H_2, and H_3 defined as

$$H_j = \left[\frac{k_z^2}{2m_l} + \frac{(-1)^j k_0 k_z}{m_l} + \frac{k_x^2+k_y^2}{2m_t} + U(z) \right] I, \quad (2)$$

$$H_3 = \begin{bmatrix} D\varepsilon_{xy} - \frac{k_x k_y}{M} & (k_y - k_x i)\Delta_{SO} \\ (-k_y - k_x i)\Delta_{SO} & D\varepsilon_{xy} - \frac{k_x k_y}{M} \end{bmatrix}. \quad (3)$$

Here j = 1, 2, I is the identity 2x2 matrix, m_t and m_l are the transversal and the longitudinal silicon effective masses, $k_0 = 0.15 \times 2\pi/a$ is the position of the valley minimum relative to the X point in unstrained silicon, ε_{xy} denotes the shear strain component, $M^{-1} \approx m_t^{-1} - m_0^{-1}$, and D = 14eV is the shear strain deformation potential. The spin-orbit term $\tau_y \otimes (k_x\sigma_x - k_y\sigma_y)$ with

$$\Delta_{so} = 2\left|\sum \frac{\langle X_1|p_j|n\rangle\langle n|[\nabla V \times p]_j|X_{2'}\rangle}{E_n - E_X}\right|, \quad (4)$$

couples states with the opposite spin projections from the opposite valleys. σ_x and σ_y are the spin Pauli matrices and τ_y is the y-Pauli matrix in the valley degree of freedom. In the Hamiltonian (1) $U(z)$ is the confinement potential, and the value Δ_{SO} = 1.27meVnm computed by the empirical pseudopotential method (Figure 1) is close to the one reported by Li and Dery (Li and Dery 2011).

3. RESULTS AND DISCUSSION

3.1. Valley splitting calculations

First we investigate the dependence of the valley splitting on the value of the potential barrier at the interfaces. The numerical results are obtained for the wave vector $\boldsymbol{k}\|[110]$ with the values k_x = 0.1nm^{-1} and k_y = 0.1nm^{-1}. Figure 2 shows the splitting for different values of the quantum well width. The valley splitting theory in SiGe/Si/SiGe quantum wells (Friesen, Chutia, Tahan, Coppersmith 2007) predicts that in the case of a symmetric square well without an electric field the valley splitting is inversely proportional to the conduction band offset ΔE_c at the interface.

However Figure 2 demonstrates clearly that the dependence is more complicated. For the quantum well of 1.36nm width the splitting first increases but later saturates. For the quantum well of 3.3nm width a significant reduction of the valley splitting around the conduction band offset value 1.5eV is observed. A further increase of the conduction band offset leads to an increase of the subband splitting value. For the quantum well of 3.3nm thickness the valley splitting saturates at about 0.17meV.

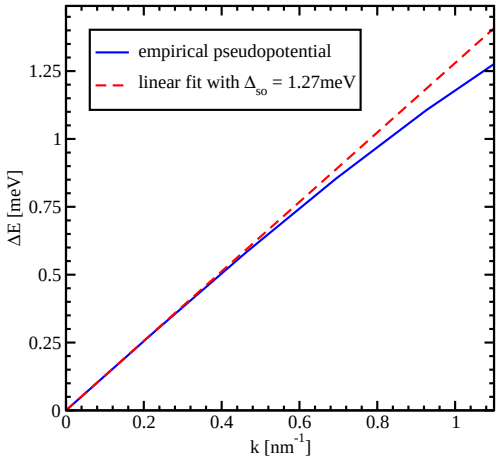

Figure 1: Empirical pseudopotential calculations of the spin-orbit interaction strength by evaluating the gap opening at the X-point between X_1 and X_2 for finite k_x

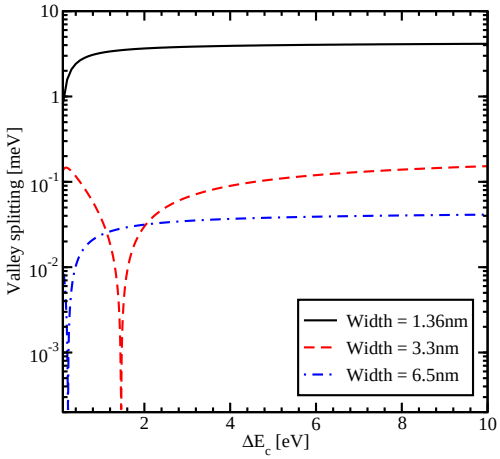

Figure 2: Splitting between the lowest unprimed electron subbands as a function of the conduction band offset at the interface for different thicknesses of the unstrained silicon film without electric field

For the quantum well of 6.5nm width a significant reduction of the valley splitting is observed for a conduction band offset value 0.2eV. The subband splitting saturates at a value 0.04meV. Although for the values of the conduction band offset smaller than 4eV the valley splitting depends on ΔE_c, for larger values of the conduction band offset it saturates indicating that the strength of the orbit-valley interaction at the interface is proportional to ΔE_c (Friesen, Chutia, Tahan, Coppersmith 2007).

The valley splitting as a function of the conduction band offset for the film of 3.3nm thickness without the electric field is shown in Figure 3. Without shear strain the valley splitting is significantly reduced around the conduction band offset value of 1.5eV. For the shear strain value of 0.25% and 0.5% the sharp reduction of the conduction subbands splitting shifts to a smaller value of ΔE_c However the region of significant

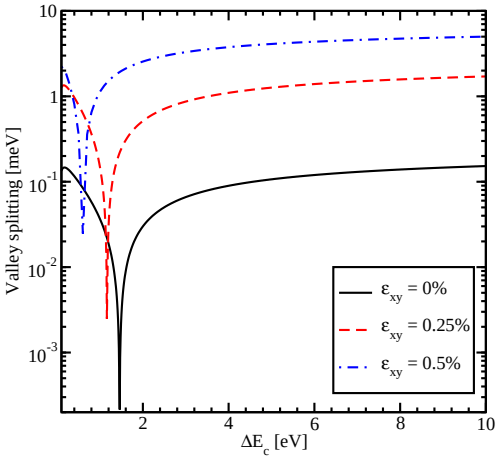

Figure 3: Valley splitting as a function of the conduction band offset for the film thickness 3.3nm without electric field

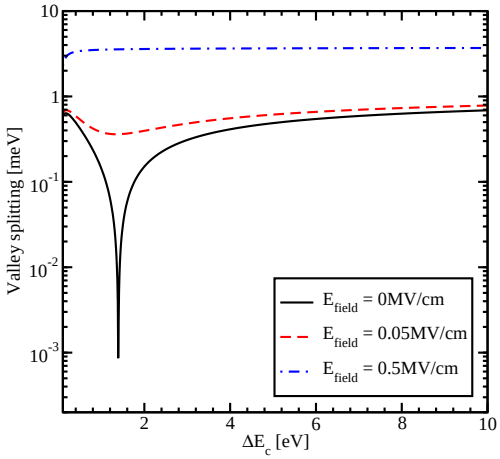

Figure 4: Dependence of the valley splitting on the conduction band offset at the interface for different values of the electric field, the shear strain value is 0.125%, and the quantum well width is 3.3nm

reduction is preserved even for the large shear strain value of 0.5%. The value of the valley splitting at saturation for large shear strain is considerably enhanced as compared to the unstrained case.

The influence of the effective electric field on the region of sharp splitting reduction is demonstrated in Figure 4. With the electric field applied the reduction in the region of interest around the conduction band offset value 1.5eV becomes smoother. However, for values of the conduction band offset smaller than 1.5eV the reduction of the valley splitting is still observed. For the values larger than 1.5eV the subband splitting slightly increases and then saturates. For the electric field value of 0.05MV/cm the saturation value of the valley splitting is almost equal to the saturated valley splitting value without electric field. For the stronger electric field of 0.5MV/cm the valley splitting reduction vanishes completely and the splitting becomes almost independent of the conduction band offset.

According to Friesen *et al.* (Friesen, Chutia, Tahan, Coppersmith 2007) the barrier height ΔE_c does not directly enter the expression of the valley splitting for a perfectly smooth interface in the presence of the electric field. The result shown in Figure 4 for the large electric field value is in a good agreement with the theory.

The splitting of the lowest unprimed electron subbands as a function of the silicon film thickness for several values of the conduction band offset at the interfaces is shown in Figure 5. The valley splitting oscillates with the film thickness increased. According to the theory (Sverdlov, Baumgartner, Windbacher, and Selberherr 2009), we generalize the equation for the valley splitting in an infinite potential square well including the spin-orbit coupling as

$$\Delta E_n = \frac{2y_n^2 B}{k_0 t\sqrt{(1-y_n^2-\eta^2)(1-y_n^2)}}\left|\sin\left(\sqrt{\frac{1-y_n^2-\eta^2}{1-y_n^2}}k_0 t\right)\right|, \quad (5)$$

with y_n, η, and B defined as

$$y_n = \frac{\pi n}{k_0 t}, \quad (6)$$

$$\eta = \frac{m_l B}{\hbar^2 k_0^2}, \quad (7)$$

$$B = \sqrt{\Delta_{so}^2\left(k_x^2 + k_y^2\right) + \left(D\varepsilon_{xy} - \frac{\hbar^2 k_x k_y}{M}\right)^2}. \quad (8)$$

Here t is the film thickness. As it was shown earlier the conduction band value of 4eV provides a subband splitting value close to the saturated one. Because Equation 5 is written for an infinite potential square well, a slight discrepancy is observed between the theoretical curve and the numerically curve calculated for the conduction band offset value 4eV in Figure 5. A large value of the conduction band offset shows better agreement between the theory and numerically obtained results.

The valley splitting as a function of the quantum well width for different values of the effective electric field is shown in Figure 6. Without electric field the valley splitting oscillates as shown in Figure 5. With electric field the oscillations are not observed in thicker films. According to Friesen *et al.* (Friesen, Chutia, Tahan, Coppersmith 2007) the condition for the independence of the valley splitting from the quantum well width is

$$\mathrm{L}^3 > \frac{2\pi^2\hbar^2}{m_l e E_{field}}. \quad (9)$$

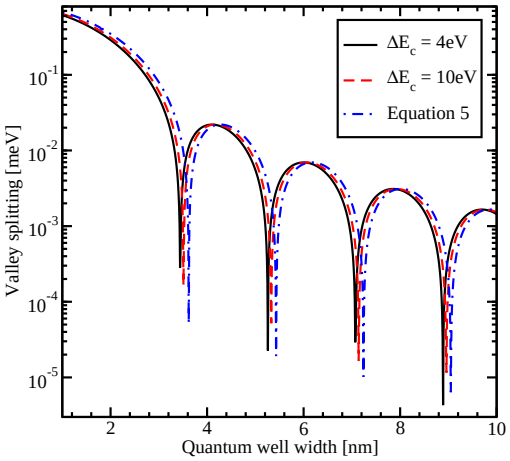

Figure 5: Splitting of the lowest unprimed electron subbands as a function of the silicon film thickness for several values of the band offset at the interface, the shear strain value is 0.05%, k_x = 0.1nm^{-1}, k_y = 0.2nm^{-1}

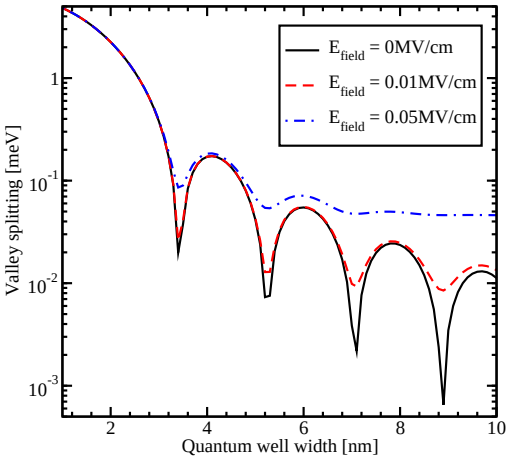

Figure 6: Splitting of the lowest unprimed electron subbands as a function of the film thickness for different values of the effective electric field, the shear strain value is 0%, the conduction band offset is 4eV, k_x = 0.1nm^{-1}, k_y = 0.1nm^{-1}

For thinner structures, the quantization is caused by the second barrier of the quantum well. The shape of the oscillations is therefore similar to that in the absence of an electric field. For the electric field of 0.05MV/cm the quantum well width should be larger than 6.9nm in order to observe the valley splitting independent on the quantum well width. This value is in good agreement with the simulation results shown in Figure 6.

We now discuss the effect of shear strain on the conduction band splitting and spin relaxation due to scattering induced by the surface roughness. The surface roughness scattering matrix elements are taken to be proportional to the square of the subband function derivatives at the interface (Fischetti, Ren, Solomon, Yang, and Rim 2003). A (001) oriented silicon film of 4nm thickness is considered, the incident wave $\boldsymbol{k}\|[510]$, the values k_x = 0.5nm^{-1}, k_y = 0.1nm^{-1}, the scattered wave $\boldsymbol{k}'\|[\bar{5}\bar{1}0]$, the values k_x' = −0.5nm^{-1}, k_y' = −0.1nm^{-1}, the spin is injected along [110] direction.

Figure 7 shows the dependence of the valley splitting on strain. Without electric field the valley splitting reduces significantly around the strain values 0.116% and 0.931% as shown in Figure 7. With electric field applied the minimum around the strain value 0.931% becomes smoother, however, for the strain value around 0.116% the sharp reduction of the valley splitting is preserved. For large electric field the valley splitting reduction around the value 0.931% vanishes completely. For the strain value 0.116% the sharp reduction of the valley splitting is still preserved at a minimum value, which is determined by the spin-orbit interaction term, only slightly affected by the electric field. As follows from Equation 5 the splitting between the subbands depends on $D\varepsilon_{xy} - \frac{\hbar^2 k_x k_y}{M}$, and the degeneracy between the unprimed subbands is increased, when this term is nonzero.

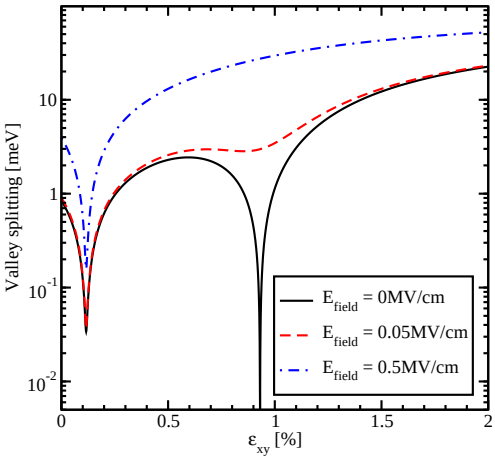

Figure 7: Splitting of the lowest conduction subbands as a function of shear strain for different values of the electric field, the quantum well thickness is 4nm, the conduction band offset is 4eV, k_x = 0.5nm^{-1}, k_y = 0.1nm^{-1}

For k_x = 0.5nm^{-1}, k_y = 0.1nm^{-1} the strain value 0.116% causes this term to vanish and minimizes the valley splitting, in good agreement with the first sharp valley splitting reduction in Figure 7. The valley splitting is also proportional to $\left|\sin\left(\sqrt{\frac{1-y_n^2-\eta^2}{1-y_n^2}}k_0 t\right)\right|$. The second minimum in the valley splitting around the strain value 0.931% in Figure 7 is because of the zero value of the $\left|\sin\left(\sqrt{\frac{1-y_n^2-\eta^2}{1-y_n^2}}k_0 t\right)\right|$ term. The effective electric field alters the confinement in the well and is therefore able to completely wash out the minimum in valley splitting due to the sine term. However, in agreement with (5), it can only slightly affect the minimum due to the shear strain dependent contribution, in agreement with Figure 7.

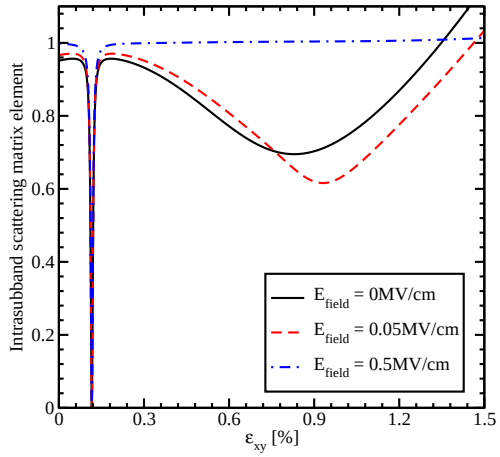

Figure 8: Intravalley scattering matrix elements normalized by their values for zero strain as a function of shear strain for different electric field values

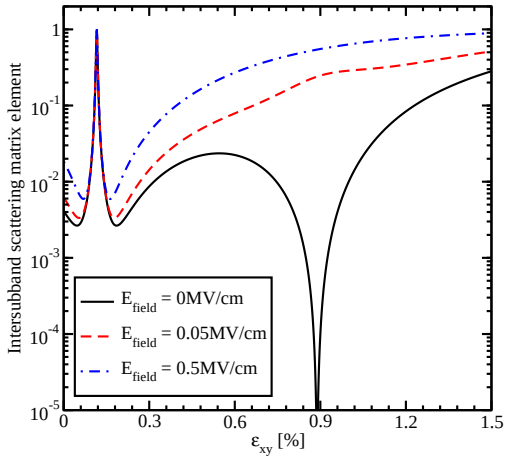

Figure 9: Intervalley scattering matrix elements normalized to the value of the intravalley scattering at zero strain as a function of strain for different electric field values

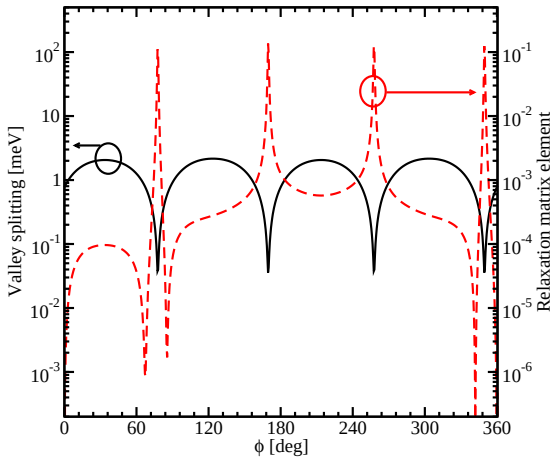

Figure 10: Dependence of the normalized spin relaxation matrix elements and valley splitting on the angle between the incident and scattered waves for the quantum well thickness is 4nm, the conduction band offset is 4eV, k_x = 0.5nm^{-1}, k_y = 0.1nm^{-1}, E_{field} = 0MV/cm, ε_{xy} = 0.01%

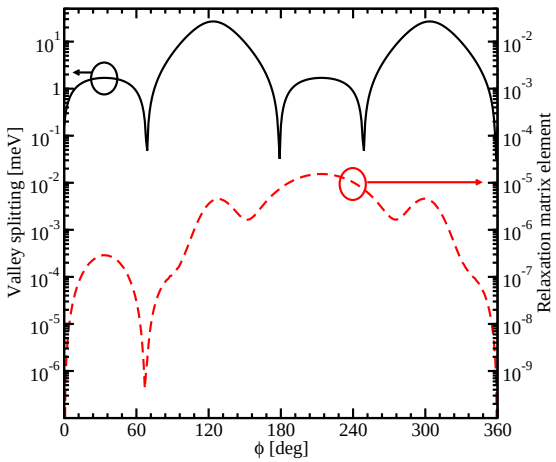

Figure 11: Dependence of the normalized spin relaxation matrix elements and valley splitting on the angle between the incident and scattered waves for the quantum well thickness is 4nm, the conduction band offset is 4eV, k_x = 0.5nm^{-1}, k_y = 0.1nm^{-1}, E_{field} = 0MV/cm, ε_{xy} = 0.92%

3.2. Scattering and relaxation matrix elements calculations

The surface roughness at the two interfaces is assumed to be equal and statistically independent. It is described by a mean and a correlation length (Fischetti, Ren, Solomon, Yang, and Rim 2003). Figure 8 and Figure 9 show the dependences on strain and electric field of the matrix elements for the intra-subband and inter-subband scattering. The intra-subband scattering matrix elements have two decreasing regions shown in Figure 8. These regions are in good agreement with the valley splitting minima in Figure 7. For higher fields the second decreasing region around the shear strain value of 0.9% vanishes. For the electric field of 0.5MV/cm the intra-subband matrix elements are sharply reduced only for the shear strain value of 0.116%. At the same time, the inter-subband matrix elements show a sharp increase around the shear strain value of 0.116%. The electric field does not affect much the valley splitting provided by the zero value of the term $D\varepsilon_{xy} - \frac{\hbar^2 k_x k_y}{M}$, and the sharp increase in the inter-subband matrix elements is observed at higher fields.

At the same time the electric field washes out and a sharp minimum around the shear strain value of 0.9% in Figure 9 occurs. With the electric field increased the confinement pushes the carriers closer to the interface which results in both inter-and intra-subband scattering matrix elements increased.

Figure 10 and Figure 11 show the sum of the inter- and intra-subband spin relaxation matrix elements (normalized to the intravalley scattering at zero strain) on the angle between the incident and scattered wave vectors simultaneously with the valley splitting calculated for the scattered wave. As shown in Figure 10, for small strain the sharp increases of the

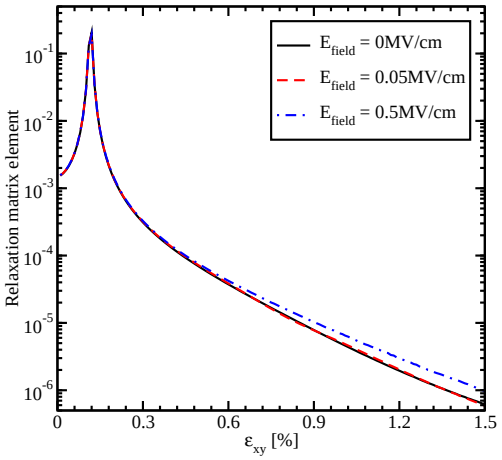

Figure 12: Spin relaxation matrix elements normalized to intravalley scattering at zero strain dependence on shear strain for several values of the electric field, k_x = 0.5nm^{-1}, k_y = 0.1nm^{-1}

relaxation matrix elements are correlated with the minima in the valley splitting, which occur for the values of the angle determined by zeroes of the $D\varepsilon_{xy} - \frac{\hbar^2 k_x' k_y'}{M}$ term. This is the condition of the formation of the so called spin hot spots characterized by spin mixing. In contrast to Figure 10, the valley splitting reduction due to the $\left|\sin\left(\sqrt{\frac{1-y_n^2-\eta^2}{1-y_n^2}}k_0 t\right)\right|$ term shown in Figure 11 does not lead to sharp increases in the spin relaxation matrix elements on the angle between the incident and scattered waves.

The dependence of the spin relaxation matrix elements shear strain for several values of the electric field is shown in Figure 12.

The spin relaxation matrix elements increase until the strain value 0.116%, the point determined by the spin hot spot condition. Applying strain larger than 0.116% suppresses spin relaxation significantly, for all values of the electric field. In contrary to the scattering matrix elements (Figure 8 and Figure 9), the relaxation matrix elements demonstrate a sharp feature only for the shear strain value of 0.116% at zero electric field. Large electric field leads to an increase of the relaxation matrix elements due to the additional field-induced confinement resulting in higher values of the surface roughness induced spin relaxation matrix elements.

3.3. Overlap calculations

In the presence of strain and confinement the four-fold degeneracy of the n-th subband is partly lifted by forming an $n+$ and $n-$ subset (the valley splitting), however, the degeneracy of the eigenstates with the opposite spin projections $n\pm\Uparrow\rangle$ and $n\pm\Downarrow\rangle$ within each subset is preserved.

The degenerate states are chosen to satisfy

$$\langle\Uparrow n \pm |f| n\pm\Downarrow\rangle = 0, \qquad (10)$$

with the operator f defined as

$$f = \cos\theta\,\sigma_z + \sin\theta\left(\cos\varphi\,\sigma_x + \sin\varphi\,\sigma_y\right), \qquad (11)$$

where θ is the polar and φ is the azimuth angle defining the orientation of the injected spin. However, the expectation value of the operator f computed between the spin up and down wave functions from the different subsets is nonzero, when the effective magnetic field direction due to the spin-orbit interaction is different from the injected spin quantization axis:

$$\bar{f} = \langle\Uparrow n \pm |f| \mp n \Downarrow\rangle \neq 0. \qquad (12)$$

Figure 13, Figure 14, and Figure 15 show the dependence of $\bar{f}$ on the orientation of the injected spin for k_x = 0.1nm^{-1}, k_y = 0.1nm^{-1} for different values of shear strain. The absolute value of the overlap $\bar{f}$ characterizes the strength of the spin up/down states mixing caused by the spin-orbit interaction. The spin mixing significantly decreases with shear strain increased in the whole range of spin orientations. This result explains the spin relaxation reduction with shear strain.

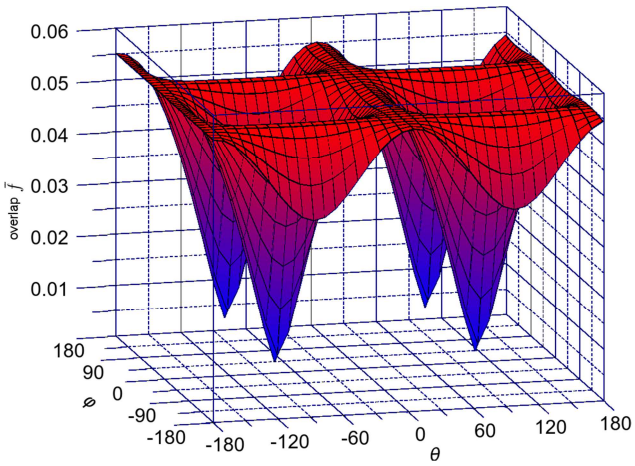

Figure 13: Dependence of the overlap of wave functions between two lowest conduction subbands on the spin injection direction for k_x = 0.1nm^{-1}, k_y = 0.1nm^{-1}, the shear strain value is 0%

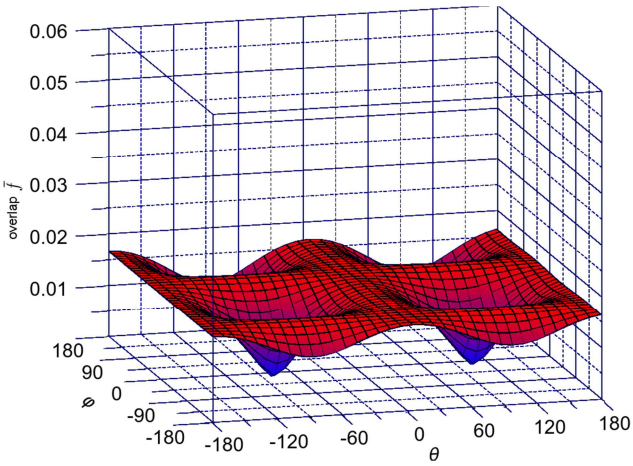

Figure 14: Dependence of the overlap of wave functions between two lowest conduction subbands on the spin injection direction for k_x = 0.1nm^{-1}, k_y = 0.1nm^{-1}, the shear strain value is 0.1%

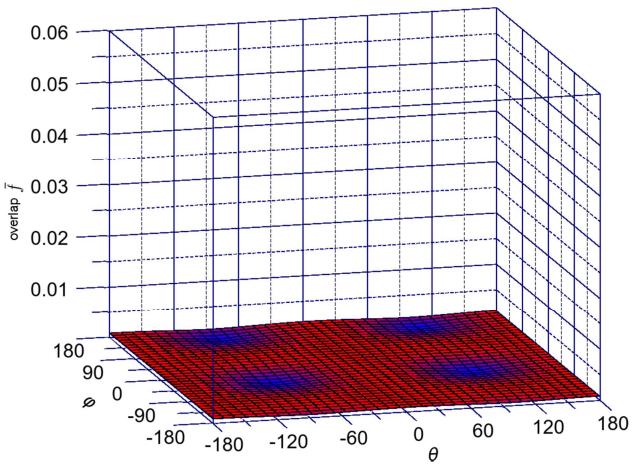

Figure 15: Dependence of the overlap of wave functions between two lowest conduction subbands on the spin injection direction for k_x = 0.1nm^{-1}, k_y = 0.1nm^{-1}, the shear strain value is 1%

4. CONCLUSION

We have investigated the lowest unprimed electron subband splitting in a thin film of a SOI-based silicon spin field-effect transistors in a wide range of parameters, including the conduction band offset at the interfaces, the width of the film, the effective electric field, and the shear strain value. We have included the spin-orbit interaction effects into the effective low-energy **k·p** Hamiltonian to investigate the valley splitting, scattering, and spin relaxation induced by the surface roughness. We have demonstrated that the valley splitting minima due to zero values of the sin-like term can be removed by the electric field, but the minimum due to a vanishing $D\varepsilon_{xy} - \frac{\hbar^2 k_x k_y}{M}$ term is preserved even for large electric fields. We have shown that, due to the inter-subband splitting increase, the matrix elements for spin relaxation decrease rapidly with shear strain. Thus, shear strain used to enhance electron mobility can also be used to boost spin lifetime.

ACKNOWLEDGMENT

This work is supported by the European Research Council through the grant #247056 MOSILSPIN

REFERENCES

Bir, G.L., Pikus, G.E., 1974. *Symmetry and strain-induced effects in semiconductors*. New York/Toronto:J. Wiley & Sons.

Cheng, J.L., Wu, M.W., Fabian, J., 2010. Theory of the spin relaxation of conduction electrons in silicon. *Physical Review Letter*, 104, 016601.

Dash, S.P., Sharma, S., Patel, R.S., de Jong, M.P., Jansen, R., 2009. Electrical creation of spin polarization in silicon at room temperature. *Nature*, 462, 491–494.

Fischetti, M.V., Ren, Z., Solomon, P.M., Yang, M., and Rim, K. 2003. Six-band k·p calculation of the hole mobility in silicon inversion layers: Dependence on surface orientation, strain, and silicon thickness. *Journal of Applied Physics*, 94, 1079.

Friesen, M., Chutia, S., Tahan, C., Coppersmith, S.N. 2007. Valley splitting theory of SiGe/Si/SiGe quantum wells. *Physical Review B*, 75, 115318.

Huang, B., Monsma, D.J., Appelbaum, I., 2007. Coherent spin transport through a 350 Micron thick silicon wafer. *Physical Review Letters*, 99, 177209.

Li, C.H., Van't Erve, O.M.J., Jonker, B.T., 2011. Electrical injection and detection of spin accumulation in silicon at 500 K with magnetic metal/silicon dioxide contacts. *Nature Communications*, 2, 245.

Li, J., Appelbaum, I., 2011. Modeling spin transport in electrostatically-gated lateral-channel silicon devices: Role of interfacial spin relaxation. *Physical Review B*, 84, 165318.

Li, P., Dery, H., 2011. Spin-orbit symmetries of conduction electrons in silicon. *Physical Review Letters*, 107, 107203.

Song, Y., Dery, H., 2012. Analysis of phonon-induced spin relaxation processes in silicon. *arXiv:1201.6660v1 [cond-mat.mtrl-sci]*. Available from: http://arxiv.org/pdf/1201.6660v1 [April 2012].

Sverdlov, V., 2011. *Strain-induced effects in advanced MOSFETs*. Wien - New York. Springer.

Sverdlov, V., Baumgartner, O., Windbacher, T., and Selberherr, S. 2009. Modeling of modern MOSFETs with strain. *Journal of Computational Electronics*, 8, 3–4.